

# NEGATIVE MUONIUM ION PRODUCTION WITH A C12A7 ELECTRIDE FILM

M. Otani\*, Y. Fukao, K. Futatsukawa, N. Kawamura, S. Matoba,  
T. Mibe, Y. Miyake, K. Shimomura, T. Yamazaki, KEK, Oho, Tsukuba, Japan  
K. Hasegawa, R. Kitamura, Y. Kondo, T. Morishita, JAEA, Tokai, Ibaraki, Japan  
T. Iijima, K. Inami, Y. Sue, M. Yotsuzuka, Nagoya University, Nagoya, Aichi, Japan  
H. Iinuma, Y. Nakazawa, Ibaraki University, Mito, Ibaraki, Japan  
K. Ishida, RIKEN, Hirosawa, Wako, Japan  
N. Saito, J-PARC Center, Tokai, Naka, Ibaraki, Japan  
H. Yasuda, University of Tokyo, Hongo, Tokyo, Japan

## Abstract

Negative muonium atom ( $\mu^+e^-e^-$ ,  $\text{Mu}^-$ ) has unique features stimulating potential interesting for several scientific fields. Since its discovery in late 1980's in vacuum, it has been discussed that the production efficiency would be improved using a low-work function material. C12A7 was a well-known insulator as a constituent of alumina cement, but was recently confirmed to exhibit electric conductivity by electron doping. The C12A7 electrider has relatively low-work function (2.9 eV). In this paper, the negative muonium production measurement with several materials including a C12A7 electrider film will be presented.

## INTRODUCTION

Negative muonium atom ( $\mu^+e^-e^-$ ,  $\text{Mu}^-$ ) has unique features catalyzing potential interesting in several scientific field. Because  $\text{Mu}^-$  is a pure leptonic system, it offers a sensitive test of quantum electrodynamics (QED) as is the case with neutral muonium atom ( $\mu^+e^-$ ,  $\text{Mu}$ ). Recently  $\text{Mu}^-$  is successfully accelerated using a radio-frequency accelerator [1]. After further acceleration and charge exchange process, an energy-variable  $\text{Mu}$  beam can be achieved. It is really new type of quantum beams and expected to open new branch of science such as antimatter gravity study [2].

$\text{Mu}^-$  has been observed in vacuum for the first time in late 1980's [3–5]. In these experiments,  $\text{Mu}^-$  is generated by injecting  $\mu^+$  to a thin target. In this method, the conversion efficiency from  $\mu^+$  to  $\text{Mu}^-$  is limited to the order of  $10^{-5}$ . Since all the potential applications need an intense  $\text{Mu}^-$ , we need to understand the  $\text{Mu}^-$  production process. It has been discussed from first  $\text{Mu}^-$  observation that the conversion efficiency would be enhanced with materials of low-work function [3, 6]. C12A7 ( $12\text{CaO}\cdot 7\text{Al}_2\text{O}_3$ ) was a well-known insulator as a constituent of alumina cement, but was recently confirmed to exhibit electric conductivity by electron doping [7]. The C12A7 electrider has lower work function (2.9 eV) than Al used in our previous experiment [8] and it is stable in atmosphere and vacuum. It was reported that nearly the same negative current signal as that with a bi-alkali material coated metal were observed in H<sup>-</sup> formation [9].

\* masashio@post.kek.jp

We have measured  $\text{Mu}^-$  intensity using several targets including a C12A7 electrider film [10]. First, we show experimental setup of the  $\text{Mu}^-$  measurement. Then, we show results of the experiment. Finally we summarize our experimental results.

## SETUP

The experiment was conducted at the Japan Proton Accelerator Research Complex (J-PARC) muon science facility (MUSE). The MUSE facility provides a pulsed  $\mu^+$  beam produced by  $\pi^+$  decay near the surface of the production target. The muon beam pulse width is approximately 40 ns in rms. The repetition rate of the beam pulse is 25 Hz [11]. For this experiment, the beam power of the J-PARC Rapid Cycle Synchrotron (RCS) was 500 kW with two bunch operations.

Figure 1 shows experimental setup for the experiment. The  $\mu^+$ s were injected to a  $\text{Mu}^-$  production target after passing through a SUS window. The thickness of the SUS window was 50  $\mu\text{m}$ . The  $\text{Mu}^-$  generated in the target was accelerated to 20 keV by the SOA electrostatic lens [12]. Then, the  $\text{Mu}^-$  was transported to the detector location via a series of electrostatic quadrupole (EQ1-4), an electrostatic deflector (ED), and a bending magnet (BM). A micro-channel plate (MCP) assembly (Hamamatsu photonics, F1217-01 [13]) detector was employed to measure time of flight (TOF) from the  $\text{Mu}^-$  production target. The  $\mu^+$  arrival time at the  $\text{Mu}^-$  production target was measured with a set of scintillating counters located at the side of the  $\text{Mu}^-$  production target.

Three types of the  $\text{Mu}^-$  target combining the Kapton foil as degrader are installed during the experiment; an Al foil, a C12A7 electrider foil, and a SUS foil. The thickness of the  $\text{Mu}^-$  production target and the Kapton foil is summarized in Table 1. The C12A7 electrider foil consists of the C12A7 electrider deposited on the Al substrate with the thickness of 200  $\mu\text{m}$ . The thickness of the C12A7 electrider deposition is approximately 10  $\mu\text{m}$ . The dimensions of the  $\text{Mu}^-$  production target were 43  $\times$  40 mm<sup>2</sup>.

The applied voltage to EQ's and ED, and the applied current to BM are tuned based on the previous experiment [14] and commissioning using H<sup>-</sup> [15]. The energy acceptance of the beamline is estimated to be 1.4% by the GEANT4 simulation [16].

Content from this work may be used under the terms of the CC BY 3.0 licence (© 2019). Any distribution of this work must maintain attribution to the author(s), title of the work, publisher, and DOI

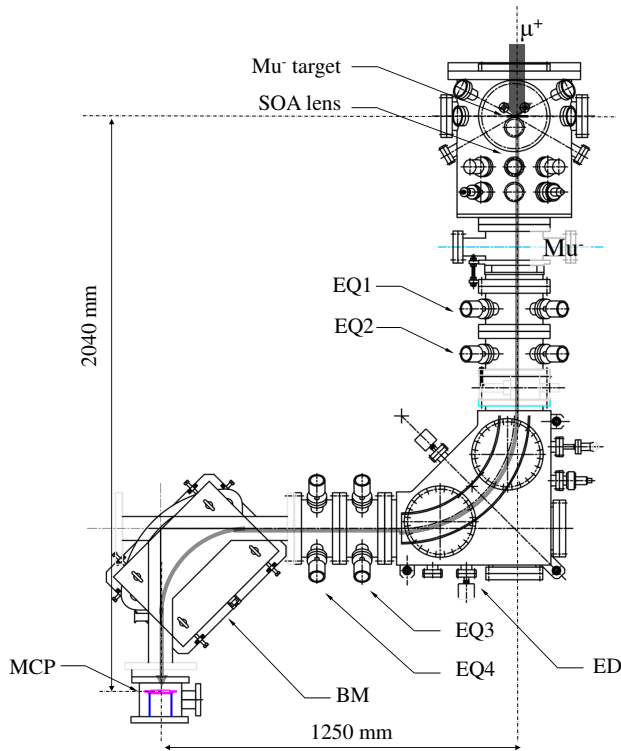


Figure 1: Schematic of the experimental setup.

Table 1:  $\text{Mu}^-$  Production Target Used in the Experiment

target	thickness	Kapton
Al	200 $\mu\text{m}$	150 $\mu\text{m}$
SUS	100 $\mu\text{m}$	75 $\mu\text{m}$
C12A7 electride	200+10 $\mu\text{m}$	150 $\mu\text{m}$

The electrical signal from the MCP was amplified using fast-filter amplifier (ORTEC 579 [17]) and digitized using CAEN V1720 [18]. The waveform in an interval of 10  $\mu\text{sec}$  around each 25-Hz beam pulse, was recorded for analysis. A pulse higher than noise level was regraded as a signal pulse. The leading edge of the signal pulse was defined as the signal timing. The pulse height is defined by the maximum height within the signal window of 40 ns.

## RESULT

Figure 2 (A) shows pulse height vs TOF for observed signal. The background events are constituted of decay positrons from muon stopped in the experimental setup and the decay positron events have lower pulse height than that of the  $\text{Mu}^-$  events [19]. After pulse height selection, the TOF distribution is obtained as shown in Fig. 2 (B). Two peaks at approximately  $-300$  ns and  $300$  ns are due to prompt positrons, that are transported through the  $\mu^+$  beamline with same momentum of  $\mu^+$ . The prompt positrons arrive earlier than  $\mu^+$  since they are faster. Blue and red curves shows fitting result assuming the decay positron background (blue) and the  $\text{Mu}^-$  signals (red). The background is consistent to

the exponential decay curve with the muon decay constant ( $\tau = 2.2 \mu\text{sec}$ ). The  $\text{Mu}^-$  peak width is consistent to that of the primary  $\mu^+$  beam. The time interval of the  $\text{Mu}^-$  peaks is consistent to that of the primary proton beam pulses. The  $\text{Mu}^-$  TOF is consistent within few percents to expectation estimated by the GEANT4 simulation where the initial energy of  $\text{Mu}^-$  is assumed to be 0.2 keV. In conclusion, we succeeded in observing the  $\text{Mu}^-$ 's.

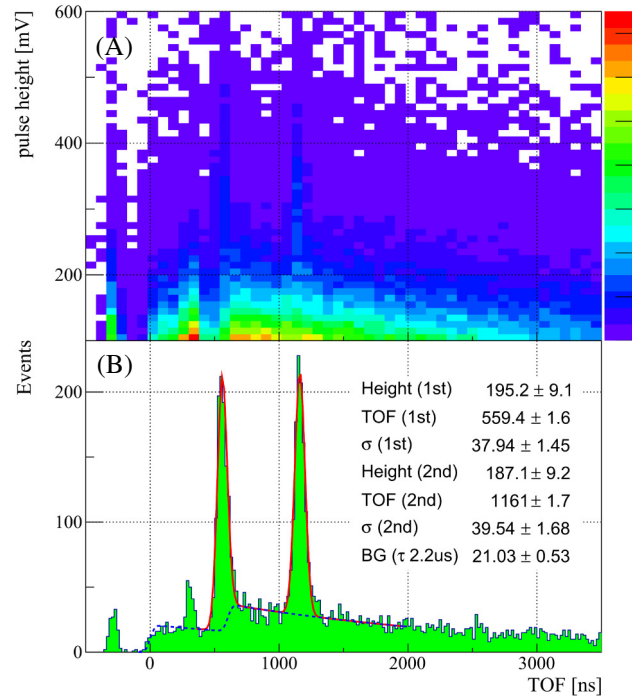


Figure 2: (A) Pulse height vs TOF for observed signal. (B) TOF distribution after pulse height selection. The red line and blue hatched line shows the fitting result assuming the  $\text{Mu}^-$  event and the decay positron background.

The  $\text{Mu}^-$  event rate is estimated by subtracting the background rate estimated by off-time region from the on-time event rate. The on-time region is defined as 440-640 ns and 1040-1240 ns. The off-time region is defined as side band regions of the on-time region.

Figure 3 shows dependence of the  $\text{Mu}^-$  event rate on the momentum of the injected  $\mu^+$  beam. The event rate is maximum for the C12A7 electride (red square) and the Al foil (blue circle) when the beam momentum is 26.2 MeV/c and 26.0 MeV/c, respectively. In this beam momentum, the half of the beam muons stopped in the target and the density of the muon stopped around the downstream surface is maximum. The  $\text{Mu}^-$  intensity is consistent within statistical uncertainty of  $\sim 10\%$  among the three targets. This systematic measurement on the input beam momentum is important input to understand the  $\text{Mu}^-$  production process. Now we are developing the Monte Carlo simulation for the  $\text{Mu}^-$  production processes based on this result.

Figure 4 shows dependence of the  $\text{Mu}^-$  event rate on acceleration voltage of the SOA lens. Because the beamline

This is a preprint — the final version is published with IOP

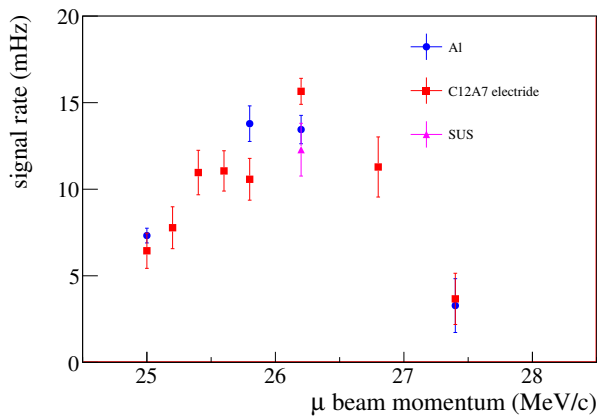


Figure 3: Dependence of the  $\text{Mu}^-$  event rate on the injected  $\mu^+$  beam momentum. Blue circle: Al foil, red square: C12A7 electride, and purple triangle: SUS foil.

setting is same except the SOA lens and the central energy of the transport beamline acceptance is 20 keV,  $\text{Mu}^-$  with an initial energy of 1 keV should be transported, for example, when the acceleration voltage is 19 keV. The energy dependence with the C12A7 electride (red square) and the Al foil (blue circle) is consistent each other within statistical error. Assuming the  $\text{Mu}^-$  energy distribution as exponential function, the average energy of the  $\text{Mu}^-$ 's is estimated to be  $0.2 \pm 0.1$  keV. It is consistent to previous experiment [3]. This result is also used for development of the Monte Carlo simulation for the  $\text{Mu}^-$  production processes.

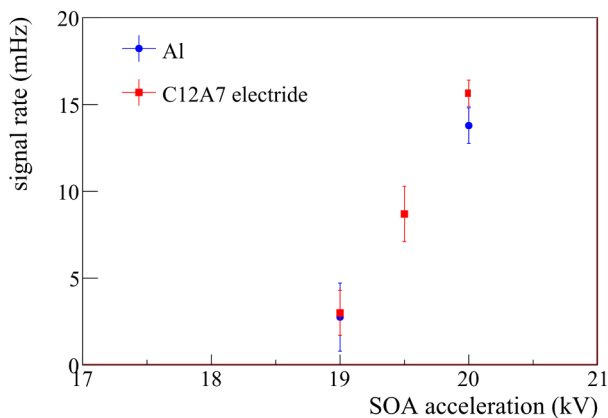


Figure 4: Dependence of the  $\text{Mu}^-$  event rate on the SOA acceleration voltage. Blue circle: Al foil, and red square: C12A7 electride

## CONCLUSION

We succeeded in measuring the  $\text{Mu}^-$  intensity with several targets including a low-work function material of the C12A7 electride. The systematic study on the momentum of the injected muon beam and the energy distribution of  $\text{Mu}^-$  emitted from the target is important input to understand the

$\text{Mu}^-$  production process. Now we are developing the Monte Carlo simulation for the  $\text{Mu}^-$  production process based on the measurement results.

## ACKNOWLEDGMENT

The experiment at the Materials and Life Science Experimental Facility of J-PARC was performed under user programs (Proposal No. 2018B0007). The authors are grateful to K. Shinto for his support in conducting the experiment. The authors would like to thank H. Hosono and T. Yokoyama for their permission to use of C12A7 electride. The C12A7 electride was supplied from AGC, and technical support by Naomichi Miyakawa, Satoru Watanabe, and Kazuhiro Ito of AGC and their discussion on data are greatly acknowledged. This work is supported by JSPS KAKENHI Grant Numbers JP25800164, JP15H03666, JP16J07784, JP16H03987, and JP18H03707.

## REFERENCES

- [1] S. Bae *et al.*, "First muon acceleration using a radio-frequency accelerator", *Phys. Rev. Accel. Beams*, 21, p. 050101, 2018.
- [2] D.M. Kaplan *et al.*, "Antimatter gravity with muonium", arxiv1601, p. 07222, 2016.
- [3] Y. Kuang *et al.*, "Formation of the negative muonium ion and charge-exchange processes for positive muons passing through thin metal foils", *Phys. Rev. A39*, p. 610, 1989.
- [4] Y. Kuang *et al.*, "First observation of the negative muonium ion produced by electron capture in a beam-foil experiment", *Phys. Rev. A35*, p. 3172, 1987.
- [5] D. R. Harshman *et al.*, "Observation of low-energy  $\mu^+$  emission from solid surfaces", *Phys. Rev. Lett.* 56, p. 2850, 1986.
- [6] V. G. Dudnikov, M. A. Cummings, R. P. Johnson, and A. V. Dudnikov, "Cold Muonium Negative Ion Production", in *Proc. 8th Int. Particle Accelerator Conf. (IPAC'17)*, Copenhagen, Denmark, May 2017, pp. 2898–2901. doi: 10.18429/JACoW-IPAC2017-WEPAB137
- [7] H. Hosono *et al.*, "High-density electron anions in a nanoporous single crystal", *Science* 301, p. 626, 2003.
- [8] R. Kitamura *et al.*, "Result of the First Muon Acceleration with Radio Frequency Quadrupole", *J. Phys.: Conf. Ser.* 874, p. 01255, 2017.
- [9] M. Sasao *et al.*, "Negative ion formation from a low-work-function nanoporous inorganic electride surface", *AIP Conf. Proc.* 1869, p. 020005, 2017.
- [10] H. Hosono, J. Kim, Y. Toda, T. Kamiya, and S. Watanabe, "Transparent amorphous oxide semiconductors for organic electronics: Application to inverted OLEDs", *Proc. Natl. Acad. Sci. USA*, 114(2), pp. 233-238, 2017.
- [11] P. Strasser *et al.*, "J-PARC decay muon channel construction status", *Journal of Physics: Conference Series* 225, 012050, 2010.
- [12] K. F. Canter, P. H. Lippel, W. S. Crane, and A. P. Mills Jr., in "Positron studies of solids, surfaces and atoms" (World Scientific, Singapore, 1986, p. 199.
- [13] Hamamatsu Photonics, K. K., <http://www.hamamatsu.com/>

- [14] P. Bakule *et al.*, “Pulsed source of ultra low energy positive muons for near-surface  $\mu$ SR studies”, *Nucl. Instr. Meth. B* 266, pp. 335-346, 2008.
- [15] Y. Nakazawa *et al.*, “Commissioning of the Diagnostic Beam Line for the Muon RF Acceleration with H- Ion Beam Derived from the Ultraviolet Light”, in *Proc. 9th Int. Particle Accelerator Conf. (IPAC'18)*, Vancouver, Canada, Apr.-May 2018, pp. 997–1000. doi:10.18429/JACoW-IPAC2018-TUPAK016
- [16] Geant4, <http://geant4.cern.ch/>
- [17] ORTEC 579., <https://www.ortec-online.com/products/electronics/amplifiers/579>
- [18] CAEN V1720., <https://www.caen.it/products/v1720/>
- [19] B. Kim *et al.*, “Development of a microchannel plate based beam profile monitor for a re-accelerated muon beam”, *Nucl. Instr. and Meth. in Phys. Res. Sec. A*, 899, p. 22, 2018.